Wavelets for Contrast Enhancement of Digital Mammography

Andrew Laine, Jian Fan and Wuhai Yang
Department of Computer and Information Science and Engineering, University of Florida

Breast cancer currently accounts for 32% of cancer incidence and 18% of cancer mortality for women in the United States. There were 182,000 new cases of breast cancer in the United States in 1993 and 46,000 deaths. Five year survival rates are generally very high (93%) for breast cancer staged as being localized, falling to 72% for regional disease and only 18% for distant disease [1]. The early detection of breast cancer is clearly a key ingredient for any strategy designed to reduce breast cancer mortality.

Despite advances in resolution and film contrast, check screen/film mammography remains a diagnostic imaging modality where image interpretation is very difficult. Breast radiographs are generally examined for the presence of malignant masses and indirect signs of malignancy, such as the presence of microcalcifications and skin thickening. Unfortunately, it is unlikely that major improvements in imaging performance will be achieved by technical advances in screen/film radiography alone. It has been suggested that as normally viewed, mammograms display only about 3% of the information they detect! [4]. The major reason for poor visualization of small malignant masses is the minor difference in x-ray attenuation between normal and malignant glandular tissues [2]. This fact makes the detection of small malignancies difficult, especially in younger women who have denser breast tissue. Although calcifications have high inherent attenuation properties, their small size results in low subject contrast [3]. As a result, the visibility of small tumors and any associated microcalcifications will always be a problem in mammography as currently performed with analog film.

Digital image processing techniques have been applied previously to mammography. The focus of past investigations has been to enhance mammographic features while reducing the enhancement of noise. Gordon and Rangayyan [5] used adaptive neighborhood image processing to enhance the relevant contrast features. This method enhanced the contrast of mammographic features as well as noise and digitization effects. Dhawan, et al. [6, 7, 8], made significant contributions towards solving problems encountered in mammographic image enhancement. They developed an adaptive neighborhood-based image processing technique that utilized low-level analysis and knowledge about a desired feature in the design of a contrast enhancement function to for specific features. Recently, Tahoces, et al. [9], developed a method for the enhancement of chest and breast radiographs by automatic spatial filtering. They used a linear combination of an original image and two smoothed images followed by nonlinear contrast stretching. Thus, spatial filtering for enhanced edges was accomplished while minimally amplifying noise.

Brzakovic, et al. [10], developed an automated system for the detection and classification of particular types of tumors in digitized mammograms. Their system identified regions corresponding to possible tumors by using multiscale image processing based on fuzzy pyramid linking. Regions were classified by means of deterministic or Bayes classifier and several metrics. They concluded that their system was very useful in detecting regions that need further analysis, but was somewhat less reliable in recognition.

Chan, et al. [11, 12], investigated the application of computer-based methods for the detection of microcalcifications in digital mammograms. Their system was based on a difference-image technique in which a signal-suppressed image was subtracted from a signal-enhanced image to remove the background in a mammogram. Signal-extraction techniques adapted to the known physical characteristics of microcalcifications were used to isolate them from the remaining noise background. They found that their method could achieve a true-positive cluster detection

 0739-5175/95/$4.00©1995

rate of approximately 80% at a false-positive detection rate of one cluster per image.

In an earlier study related to this paper, computer simulated images were used to optimized multiscale wavelet based processing techniques [13]. Mathematical phantom images contained a Gaussian-shaped signal in half of the regions and included several levels of random noise. Signal intensity and noise levels were varied to determine a detection threshold contrast-to-noise ratio (CNR). An index of the ratio of output to input contrast to noise ratios was then used to optimized wavelet based image processing algorithms. Computed CNRs were found to correlate well with signal detection by human observers in both the original and processed images.

Our approach to feature analysis and contrast enhancement is motivated in part by recently discovered biological mechanisms of the human visual system [14]. Both multi-orientation and multiresolution are known features of the human visual system. Specifically, there exist cortical neurons which respond specifically to stimuli within certain orientations and frequencies. In this paper, we exploit the orientation and frequency selectivity of multiscale wavelet transforms to make mammographic features more obvious through localized contrast gain.

This paper is organized into two parts. In the first part we present a mathematical foundation for an approach to accomplish image contrast enhancement by multiresolution representations of the dyadic wavelet transform. We formulate two examples in which a linear enhancement operator is shown mathematically equivalent to traditional unsharp masking with a Gaussian low-pass filter. A formal analysis of wavelet filter selection and associated artifacts is carried out. Then we show that transform coefficients, modified within each level of scale by nonlinear operators, can make more obvious unseen or barely seen features of mammography without requiring additional radiation. In addition, we introduce an edge-preserved denoising stage based on wavelet shrinkage with adaptive thresholding, and demonstrate that noise suppression and contrast enhancement can be achieved simultaneously within the same framework.

In the second part, we analyze arbitrary regions of interest (ROI) of a digital mammogram by (overcomplete) Deslauriers-Dubuc interval wavelets. This could provide radiologists with an interactive capability for local processing of suspicious lesions within large image matrix sizes. We demonstrate that features extracted from this multiscale representation can support an adaptive mechanism for accomplishing local contrast enhancement. Our results are compared with traditional image enhancement techniques by measuring the local contrast of known mammographic features.

PART 1: DYADIC WAVELET ANALYSIS

Image contrast is an important factor in the subjective quality of radiographic images. A comprehensive survey of algorithms for contrast enhancement is presented in [15]. Histogram modification techniques [16, 17] have been attractive due to their simplicity and speed. A transformation function is first derived from a desired histogram and the histogram of an input image. The trans-formation function is usually nonlinear and for continuous functions, a listless transformation may be achieved. However, for digital radiographs having a finite number of gray levels, some information loss due to quatization errors is typical. For example, a subtle edge may be merged with its neighboring pixels and disappear. Methods that incorporate local context into the transformation process may also have problems. For example, simple adaptive histogram equalization [18] with a fixed contextual region (window) cannot adapt to features of distinct sizes.

Most edge enhancement algorithms share a common strategy: edge detection and subsequent "crispening." *Unsharp masking* sharpens edges by subtracting a portion of a Laplacian filtered component from an original image. This technique was justified as an approximation of a deblurring process in [19]. Loo, et al. [20], studied an extension of this technique in the context of radiographs. In addition, an extension based on Laplacian filtering was proposed in [21]. However, these (unsharp masking) techniques are limited by their linear and single scale nature, and are less effective for images containing diverse features typically found in mammography. In an attempt to overcome these limitations, a local contrast measure and nonlinear transform functions were introduced in [5], and subsequently refined in [22].

More recently, the advancement of wavelet theory has sparked researchers in the application of image contrast enhancement [23-29]. These early studies revealed promising results, but were more experimental in design. In this part, we provide a concise mathematical analysis of a dyadic wavelet transform, and reveal its connection to the traditional technique of unsharp masking. In addition, we propose a simple nonlinear enhancement function and analyze the problem of artifacts. We next describe an explicit denoising stage that preserves edges using wavelet shrinkage [33] with adaptive thresholding. In addition, we present a two-dimensional extension for digital mammography and special procedures developed for accomplishing denoising and enhancement without orientation distortion. Finally, sample results are shown and comparisons made using both digitalized mammograms and synthetic signals.

One-dimensional Discrete Dyadic Wavelet Transform

A fast algorithm [31] for computing 1-D discrete dyadic wavelet transform (DDWT) is shown in Fig. 1. The left side

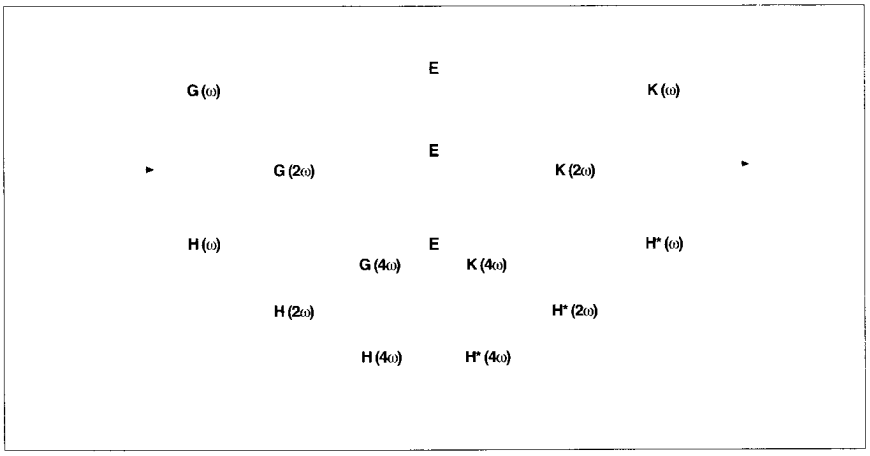

1. One dimensional discrete dyadic wavelet transform (three levels shown).

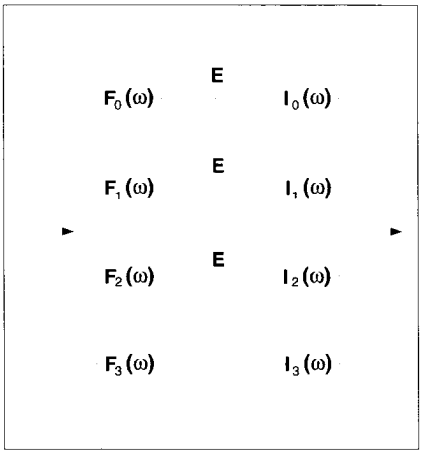

2. An equivalent multi-channel structure for three-level DDWT.

shows the structure of decomposition, and the right, reconstruction. For an N-channel structure, there are $N-1$ high-pass or band-pass channels and a low-pass channel. Thus, the decomposition of a signal produces $N-1$ sets of wavelet coefficients and a coarse signal. In Fig. 1, decomposition filters differ from reconstruction filters. However, this structure is equivalent to the multichannel structure shown in Fig. 2. This computational structure makes obvious the potential for parallel processing to support an interactive user interface for computed assisted diagnosis.

Channel frequency responses $C_m(\omega)$ can be written as:

$$C_m(\omega)=F_m(\omega)I_m(\omega)=$$
$$\begin{cases}1-\|H(\omega)\|^2 & m=0\\ \prod_{l=0}^{m-1}\|H(2^l\omega)\|^2\left[1-\|H(2^m\omega)\|^2\right] & 1\le m\le(N-1)\\ \prod_{l=0}^{N-1}\|H(2^l\omega)\|^2 & m=N\end{cases}$$

As an example, we consider an extension of the class of filters proposed in [31]:

$$H(\omega)=e^{jp\frac{\omega}{2}}\left[\cos\left(\frac{\omega}{2}\right)\right]^{2n+p} \quad (1)$$

where $p=0$, or 1. Let:

$$\Theta_{m,q}(\omega)=\left[\prod_{l=0}^{m-1}\cos\left(2^{l-1}\omega\right)\right]^q$$

then we can show that:

$$\Theta_{m,q}(\omega)=\left[\frac{\sin\left(2^{m-1}\omega\right)}{2^m\sin\left(\frac{\omega}{2}\right)}\right]^q \quad (2)$$

and therefore:

$$c_m(\omega)=$$
$$\begin{cases}\Theta_{m,4n+2p}(\omega)-\Theta_{m+1,4n+2p}(\omega), & 0\le m\le(N-1)\\ \Theta_{N,4n+2p}(\omega), & m=N\end{cases} \quad (3)$$

Note that $\Theta_{0,n}(\omega)=1$, and for $0<m<N$

$$C_m(\omega)=\Theta_{m,4n+2p}(\omega)-\Theta_{m+1,4n+2p}(\omega)$$
$$=\sin^2\left(\frac{\omega}{2}\right)4^m\Theta_{m,4n+2p+2}(\omega)$$
$$\sum_{l=0}^{2n+p-1}\left[\cos\left(2^{m-1}\omega\right)\right]^{2l}$$

and $\sin^2\left(\frac{\omega}{2}\right)$ is the frequency response of the discrete Laplacian operator having an impulse response of $\{1;\ -2;\ 1\}$.

$\Theta_{m,q}(\omega)$ with even exponential q is approximately a Gaussian function, while the frequency responses of channels ($0<m<N$) are approximately a Laplacian of Gaussian.

Linear Enhancement and Unsharp Masking

Review of Unsharp Masking

A prototype of unsharp masking can be defined [19] as:

$$\tilde{s}(x,y)=s(x,y)-k\Delta s(x,y) \quad (4)$$

where $\Delta=\frac{\partial^2}{\partial x^2}+\frac{\partial^2}{\partial y^2}$ is the Laplacian operator. However, this original formula processed only the level of finest resolution. More versatile formulas were later fashioned in two forms, described below.

One way to extend the original formula was based on exploiting the averaging concept behind the Laplacian operator. The discrete form of the Laplacian operator may be written as:

$$\Delta s(i,j)=\left[s(i+1,j)-2s(i,j)+s(i-1,j)\right]$$
$$+\left[s(i,j+1)-2s(i,j)+s(i,j-1)\right]$$
$$=-5\left\{s(i,j)-\frac{1}{5}\left[s(i+1,j)+s(i-1,j)\right.\right.$$
$$\left.\left.+s(i,j)s(i,j+1)+s(i,j-1)\right]\right\}$$

This formula shows that the discrete Laplacian operator can be implemented by subtracting from the value of a central point its average neighborhood. Thus, an extended formula [20] can be written as:

$$\tilde{s}(i,j)=s(i,j)+k\left[s(i,j)-s(i,j)*h(i,j)\right] \quad (5)$$

where $h(i,j)$ is a discrete averaging filter, and * denotes convolution. For example, in [20] an equal-weighted averaging mask was used:

$$h(x,y)=\begin{cases}1/N^2, & |x|<n/2,|y|<n/2\\ 0, & \text{otherwise.}\end{cases}$$

Another way to extend the prototype formula [21] came from the idea of a Laplacian-of-Gaussian filter, which expands Equation (4) into:

$$\tilde{s}(x,y)=s(x,y)-k\Delta\left[s(x,y)*g(x,y)\right]$$
$$=s(x,y)-k\left[s(x,y)*\Delta g(x,y)\right] \quad (6)$$

where $g(x,y)$ is an Gaussian function, and $\Delta g(x,y)$ is a Laplacian-of-Gaussian filter.

Finally, we mention that both extensions (Eqs. (5) and (6)) are limited to a single scale.

Unsharp Masking is Included Within a DDWT Framework

Next, we prove that unsharp masking with a Gaussian lowpass filter can be included in a dyadic wavelet framework for enhancement by considering two special cases of linear enhancement.

In the first case, transform coefficients of channels $0\le m\le N-1$ are enhanced (multiplied) by the same gain $G_0>1$, or $G_m=G_0>1$, $0\le m\le N-1$. The system frequency response is thus:

$$V(\omega)=\sum_{m=0}^{N-1}G_mC_m(\omega)+C_N(\omega)$$
$$=G_0\sum_{m=0}^{N}C_m(\omega)-(G_0-1)C_N(\omega)$$
$$=G_0-(G_0-1)C_N(\omega)$$
$$=1+(G_0-1)\left[1-C_N(\omega)\right]$$

The input-output relationship of the system is then simply:

$$\tilde{s}[i]=s[i]+(G_0-1)\left\{s[i]-s[i]*c_N[i]\right\} \quad (7)$$

Since $C_N(\omega)$ is approximately a Gaussian lowpass filter, Eq. (7) may be seen as the 1-D counterpart of Eq. (5).

In the second case, transform coefficients of a single channel p, $0\le p\le N$ are enhanced (multiplied) by a gain $G_p>1$, thus:

$$V(\omega)=\sum_{m\ne p}C_m(\omega)+G_pC_p(\omega)$$
$$=\sum_{m=0}^{N}C_m(\omega)+(G_p-1)C_p(\omega)$$
$$=1+(G_p-1)C_p(\omega) \quad (8)$$

Using the filter class of Eq. (1), the input-output relationship of the system defined in Eq. (8) can be written as:

$$\tilde{s}[i] = s[i] - (G_p - 1) \cdot \Delta\{s[i] * \beta[i]\} \quad (9)$$

where $\beta[i]$ is the impulse response of an approximate Gaussian filter. Similarly, Eq. (9) may be seen as the 1-D counterpart of Eq. (6). The inclusion of these two forms of unsharp masking clearly demonstrate the flexibility and versatility of this dyadic wavelet framework.

Figure 3 shows an example of linear enhancement using uniform gains across scales. This example clearly demonstrates an increase of local contrast marked by a steeper slope and localized emphasis (undershooting and overshooting). Note that the observed undershooting and overshooting associated with the strong edge is much larger than that of the weaker edge. Therefore, linear enhancement techniques are especially well suited for the enhancement of microcalcifications.

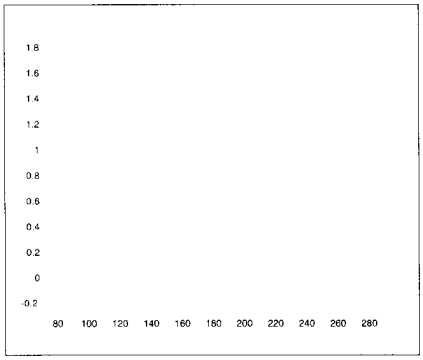

3. Three level linear enhancement (solid line) for G_m = 10, overlayed with the original signal (dotted line).

Nonlinear Enhancement by Functional Mapping

However, linear enhancement tends only to emphasize strong edges, which can lead to inefficient usage of the dynamic range available on a display screen. For example, mammograms enhanced by a linear operator containing a single obvious (high intensity) macrocalcification will result in gross rescaling within the available dynamic range of a display. This makes the detection of subtle features of importance to mammography more difficult. Below, we show how this problem may be solved by a simple nonlinear method. Linear enhancement can be seen as a mapping of wavelet coefficients by a linear function $E_m(x) = G_m x$. A direct extension of linear enhancement is a nonlinear mapping function, described next.

Filter Selection and Enhancement Function Design

For linear enhancement, selection of the filters $G(\omega)$ (and thus $K(\omega)$) make little difference. However, the selection of filters is critical for the nonlinear case. We chose a discrete Laplacian operator as the filter $G(\omega)$. A discrete Laplacian operator can be implemented by the filter:

$$G(\omega) = -4\left[\sin\frac{\omega}{2}\right]^2, \text{ or } g[n] = \{1, -2, 1\}$$

such that $g[n] * s[n] = s[n+1] - 2s[n] + s[n-1]$.

In addition, both filters $H(\omega)$ and $K(\omega)$ can be symmetric:

$$H(\omega) = \left[\cos\left(\frac{\omega}{2}\right)\right]^{2n},$$

$$\text{and } K(\omega) = \frac{1 - \|H(\omega)\|^2}{G(\omega)} = -\frac{1}{4}\sum_{l=0}^{2n-1}\left[\cos\left(\frac{\omega}{2}\right)\right]^{2l}$$

Our guidelines for designing a nonlinear enhancement function were:

(1) An area of low contrast should be enhanced more than an area of high contrast. This is equivalent to saying that small values of $w_m[i]$ should be assigned larger gains.

(2) A sharp edge should not be blurred.

In addition, an enhancement function may be further subjected to the constraints:

(1) Monotonicity, in order not to change the position of local extrema, nor create new extrema.

(2) Antisymmetry, $E(-x) = -E(x)$, in order to preserve phase polarity for "edge crispening."

A simple piecewise linear function that satisfies these conditions is shown in Figure 4:

$$E(x) = \begin{cases} x - (K-1)T, & \text{if } x < -T \\ Kx, & \text{if } |x| \le T \\ x + (K-1)T, & \text{if } x > T \end{cases} \quad (10)$$

where $K > 1$. Note that for $T \ge \max\{|w[n]|\}$, each wavelet coefficient will be multiplied by a gain of K_0, reducing the function to a linear function. This implies that our nonlinear algorithm includes unsharp masking as a subset.

Threshold Selection

For each level m, an enhancement operator E_m has two parameters: threshold T_m and gain K_m. In our experimental studies, gain was the same value across

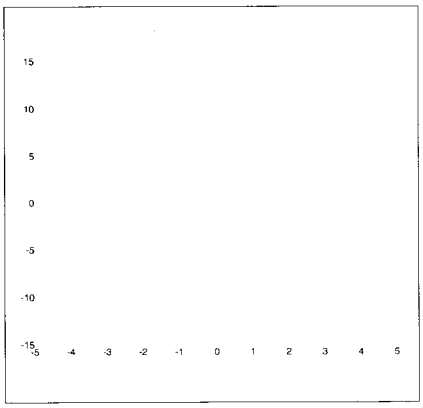

4. Enhancement function $E(x)$, for T = 0.5 and K = 20.

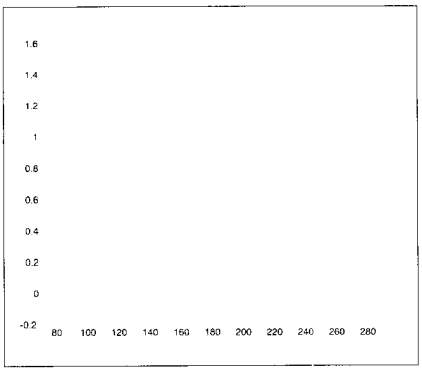

5. 1-D contrast enhancement by three-level dyadic wavelet analysis with a nonlinear operator, t = 0.06 and G_m = 20. (solid line: enhanced signal; dotted line: original signal).

levels, such that $K_m = K_0$; $0 \le m \le N-1$, and T_m was set in two distinct ways, according to the two considerations mentioned earlier in this section.

(1) For the purpose of enhancing weak features, we set threshold $T_m = t \times \max\{|w_m[n]|\}$, where $0 < t < 1$ was user specified. By setting a small t across levels, we assured that weak features at distinct scales were always favored and effectively enhanced. Figure 5 shows a numerical example of nonlinear enhancement. Note that enhancement of both edges is accomplished (especially the weak edge).

(2) To make efficient use of the dynamic range of the computer screen, thresholds were bound in the following way: At each level, the magnitudes of wavelet coefficients were quantized into 1024 bins, and a distribution (histogram) h was computed. For a user specified t, $0 < t < 1$, an actual threshold T_m was computed such that

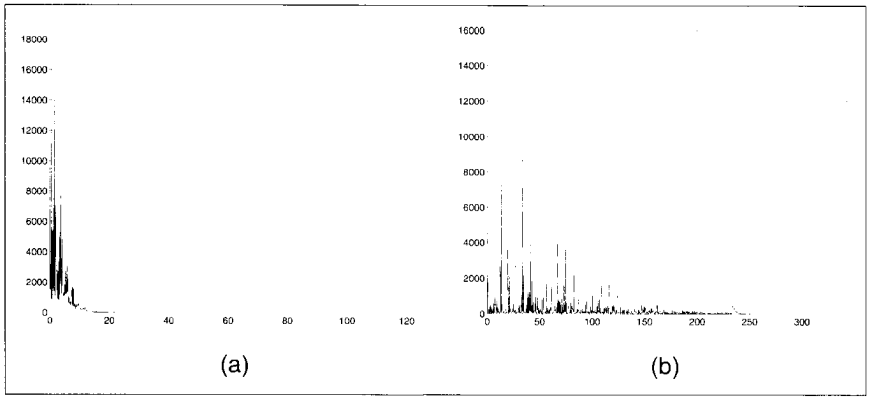

6. (a) Distribution of wavelet coefficient magnitudes for level 1. (b) Distribution of wavelet coefficient magnitudes after enhancement processing (t = 0.002 and G = 20).

$\left(\sum_{n=k}^{N-1} h[n]\right) / \left(\sum_{n=0}^{N-1} h[n]\right) \approx t$. Thus, the threshold T_m divided the range of wavelet coefficients into two regions. The region with values larger than the threshold T_m was then compressed, and the lower region stretched. Figure 6 shows a sample result for the digital mammogram exhibited in Fig. 10 (a).

We claim that our multiscale algorithm provides a marked improvement over traditional techniques in two respects:

1. The efficient multiscale (or multimask) decomposition localizes searches for features existing within distinct scales, making the traditional "try-and-fail" strategy of window selection unnecessary.

2. The nonlinear algorithm enhances small features within each scale without blurring the edges of larger features. Thus making possible the simultaneous enhancement of features of various size.

Furthermore, artifacts possibly created by a nonlinear enhancement operator can be limited by judicious selection of filters and design constraints. For example, the arguments presented below assure that no new extrema (artifacts) will be created within each channel.

1. Filters are zero-phase. No spatial shifting of features exists in the transform space.

2. $E(x)$ is a monotonically increasing function, and thus will not produce new extrema points.

3. The reconstruction filters are simply zero-phase smoothing filters.

The nonlinear enhancement methods described above do not take into account the presence of noise. In general, noise exists in a digitized image due to the imaging device and quantization. As a result of nonlinear processing, noise may be amplified and may diminish the benefits of contrast enhancement. In the next section, we present a method to accomplish denoising.

Incorporating Denoising into Enhancement

Unfortunately, denoising is a very difficult problem. Fundamentally, there is no absolute boundary to distinguish a feature from noise. Even if there are known characteristics for a particular type of noise, it may be theoretically impossible to completely separate the noise from features of interest. Therefore, denoising methods may be seen as ways to suppress very high frequency and incoherent components of an input signal.

A very simple method of denoising that is equivalent to low-pass filtering is naturally included in a dyadic wavelet framework. That is, simply discard several channels of high spatial frequency, and enhance channels of lower frequency. The problem associated with this linear denoising approach is that edges are blurred significantly, rendering it unsuitable for contrast enhancement. In order to achieve edge-preserved denoising, more sophisticated methods based on wavelet analysis have been proposed. Mallat and Hwang [32] connected noise behavior to singularities. Their algorithm was based on a multiscale edge representation. The algorithm traced modulus wavelet maxima to evaluate local Lipschitz exponents and deleted maxima points with a negative Lipschitz value. In addition, Donoho [33] proposed nonlinear wavelet shrinkage. This algorithm reduced wavelet coefficient values towards zero, based on a level-depedent threshold.

A denoising stage based on wavelet shrinkage can be incorporated into our enhancement algorithm. However, there are two arguments which favor shrinking gradient coefficients instead of Laplacian coefficients [34].

In the previous section, we argued that nonlinear enhancement should be performed on Laplacian coefficients. Therefore, in order to incorporate denoising into our enhancement algorithm, we split the Laplacian operator into two cascaded gradient operators. Note that:

$$G_m(\omega) = -4\left[\sin\left(2^{m-1}\omega\right)\right]^2 = \begin{cases} \left[e^{-j\omega/2} G_d\left(\frac{\omega}{2}\right)\right]\left[e^{j\omega/2} G_d\left(\frac{\omega}{2}\right)\right] & \text{if } m = 0 \\ \left[G_d\left(2^{m-1}\omega\right)\right]^2 & \text{otherwise} \end{cases} \tag{11}$$

where $G_d(\omega) = 2j \sin(\omega)$.

Denoising by wavelet shrinkage [33] can then be incorporated into this structure, as illustrated in Fig. 7, where the shrinking operator can be written as:

$$C(x) = sign(x) \cdot \begin{cases} |x| - T_n & \text{if } |x| > T_n, \\ 0 & \text{otherwise.} \end{cases}$$

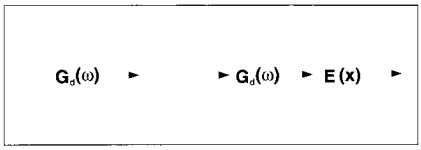

7. Incorporating wavelet shrinkage into an enhancement framework (level one shown).

For our application to digital mammography, we have chosen a shrinking operator that is a piece-wise linear and monotonically non-decreasing function, which will not introduce artifacts.

Two Dimensional Extension

For processing digital mammograms, the one-dimensional structures presented above were simply extended for two dimensions. We first adopted the method proposed by Mallat [31], shown in Fig. 8, where filter $L(\omega) = \frac{1 + |H(\omega)|^2}{2}$, and $H(\omega)$, $K(\omega)$ and $G(\omega)$ were the same filters used in the 1-D case.

However, experimentally we observed that if we simply modified the two oriented wavelet coefficients independently, orientation distortions were introduced.

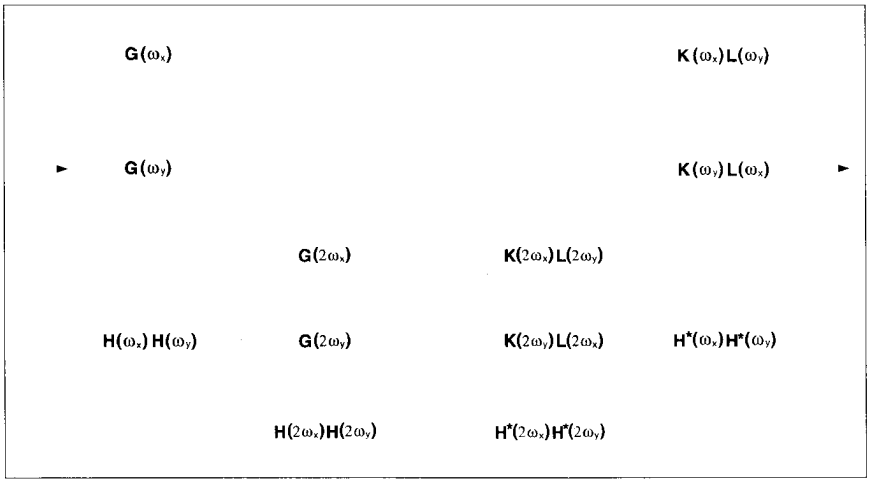

8. Two-dimensional dyadic wavelet transform (two levels shown).

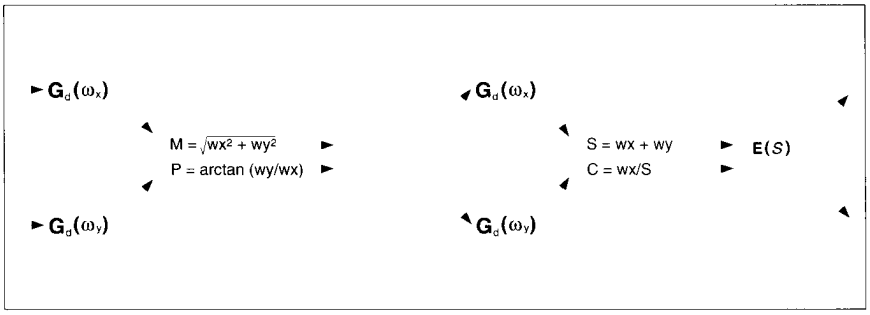

9. Denoising and enhancement for the 2-D case (level one shown).

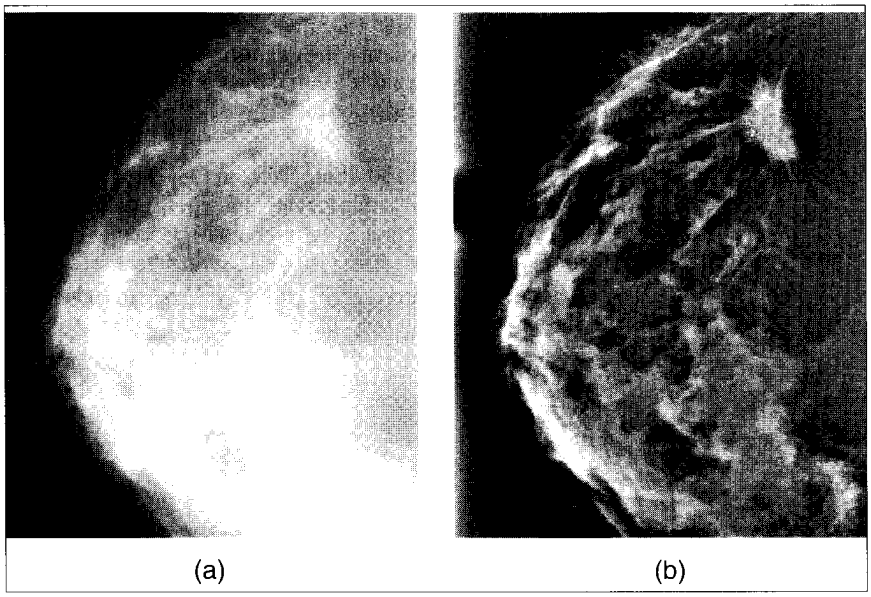

10. (a) Original mammogram M63. (b) Nonlinear enhancement with denoising, N = 5, G_m = 20, t = 0.02 (Type 2 thresholding).

These potentially disastrous artifacts were avoided by applying a denoising operation to the magnitude of gradient coefficients, and then applying a nonlinear enhancement operation on the sum of the Laplacian coefficients, as shown in Fig. 9. For the two oriented gradient coefficients wx_1 and wy_1, the magnitude M and phase P were computed as $M = \sqrt{wx_1^2 + wy_1^2}$ and $P = \arctan(wy_1/wx_1)$, respectively. The denoising operation was then applied to M, obtaining M'. The denoised coefficients were then simply restored as $wx'_1 = M'^* \cos(P)$ and $wy'_1 = M'^* \sin(P)$, respectively. For the enhancement operation, notice that the sum of two Laplacian components is *isotropic*. Therefore, we computed the sum of the two Laplacian components as $S = wx_2 + wy_2$ and $C = wx_2/S$. A nonlinear enhancement operator was then applied to S only, producing S'. Thus, the two restored components were $wx'_2 = S' * C$ and $wy'_2 = S' * (1 - C)$.

Experimental Results

In this section, we present some samples of our experimental results. Film radiographs of the breast were digitized using a sampling size of 210 microns, on a Kodak laser film digitizer, with 10-bit quantization (contrast resolution).

Figure 10 (a) shows a digital mammogram of size 400x512 containing a stellate lesion. Figure 10 (b) shows a nonlinear enhancement of the radiograph. The structure of the lesion is more clearly shown, as well as the boundary tissue of the breast. The local effect of contrast enhancement can be appreciated more precisely by the detail of the scan line comparison shown in Fig. 11.

Figure 12 (a) shows a digital mammogram of size 512x512 containing stellate lesions. Figure 12 (b) shows the image after processing by nonlinear enhancement. The structure and borders of the lesions are well defined, as are the vascular, nipple and glandular tissues. The benefit of contrast enhancement can be seen by the subtle variations of the scan line profile compared in Fig. 13.

PART 2: INTERVAL WAVELETS

We next describe a method for accomplishing an interactive paradigm for adaptive contrast enhancement [23-26, 28]. In this study, we have investigated Deslauriers-Dubuc interpolation wavelets [35, 36] constructed on the interval to compute a multiscale representation. Mammograms were reconstructed from transform coefficients modified at each level by local and global nonlinear operators. This representation was attractive because it subdued the "edge effects" of traditional multiresolution representations (based on perodization of a finite signal to a signal on a line; or simply adding zeros to extend a signal on a line). The shape of the basis functions for these representations can be

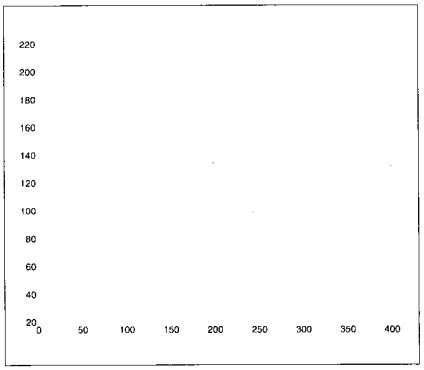

11. Sample horizontal scan line from M63 (107 pixels from the top) comparing enhancement with original profile (dotted line: original, solid line: enhanced)

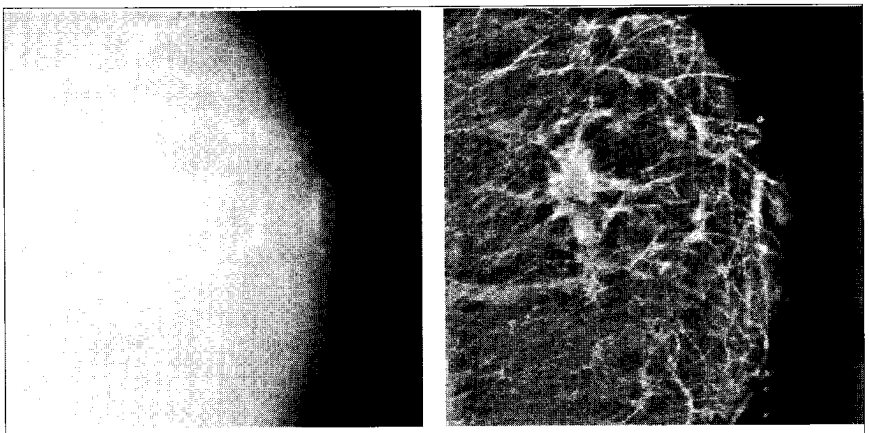

12. (a) Original mammogram image M87. (b) Nonlinear enhancement with denoising, $N = 5$, $G_m = 20$, $t = 0.1$ (Type 1 thresholding).

symmetric or antisymmetric, and allow for perfect reconstruction. In this paper, we applied this analysis to decompose an arbitrary region of interest of a mammogram, so that a selected region could be analyzed independent of its surrounding context.

In many applications, a signal has finite length, such that the signal lives on the interval [0, 1], or in the two-dimensional case, an image. Cohen and Daubechies [37] and Jawerth [40] adapted multiresolution analysis on the line to "life on the interval," where a sequence of successive approximation spaces on the interval were constructed as:

$$\overline{\cup_{j\in\mathbf{Z}} V_j} = \mathbf{L}^2[0,1], \cap_{j\in\mathbf{Z}} V_j = \{0\}.$$

By defining W_j as an orthogonal complement of V_j in V_{j-1}, $V_{j-1} = V_j \oplus W_j$, the space $\mathbf{L}^2$ [0, 1] can be represented as a direct sum $\mathbf{L}^2$ [0, 1] = $\oplus_{j\in\mathbf{Z}} W_j$.

Deslauriers-Dubuc Interpolation

In this study, we investigated multiresolution representations of the Deslauriers-Dubuc fundamental functions [35, 36]. Figure 14 shows a fundamental solution of Deslauriers-Dubuc interpolation and its associated wavelet ($D = 3$).

Donoho [38] showed how to adapt the Deslauriers-Dubuc interpolating transform to "life on the interval." Suppose that $\phi_{j,k}$ is a scaling function on the line. The scaling functions on the interval $\psi_{j,k}^{interv}$ can be derived as follows:

(1) Within the interior of the interval, they are simply the same as on the real line:

$$\phi_{j,k}^{interv} = \phi_{j,k}, \quad D < k < 2^j - D - 1$$

(2) On the *edges* of the interval, they are dialations of the boundary adjusted functions:

$$\phi_{j,k}^{interv} = 2^{j/2}\phi_k^{left}\left(2^j x - k\right), 0 \le k \le D, \text{ and}$$
$$\phi_{j,2^j-k-1}^{interv} = 2^{j/2}\phi_k^{right}\left(2^j x - 2^j - k - 1\right),$$
$$\text{for } 0 \le k \le D$$

Thus for the spaces V_j[0, 1] we can define the functions:

$$\phi_{j,k}^{interv} = \begin{cases} \phi_{j,k}^{left} & 0 \le k \le D \\ \phi_{j,k} & D < k < 2^j - D - 1 \\ \phi_{j,k}^{right} & 2^j - D - 1 \le k \le 2^j \end{cases}$$

Similarly, we can construct wavelets on the interval for the detail spaces W_j[0, 1]:

$$\psi_{j,k}^{interv} = \begin{cases} \psi_{j,k}^{left} & 0 \le k < \lfloor D/2 \rfloor \\ \psi_{j,k} & \lfloor D/2 \rfloor \le k < 2^j - \lfloor D/2 \rfloor \\ \psi_{j,k}^{right} & 2^j - \lfloor D/2 \rfloor \le k < 2^j \end{cases}$$

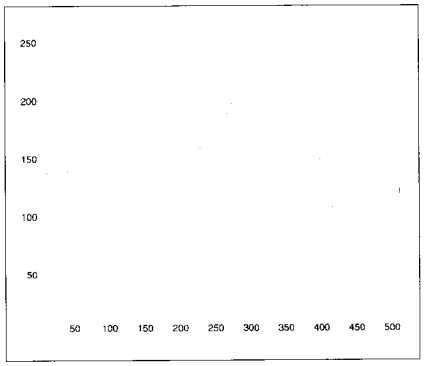

13. Sample horizontal scan line from M87 (located 210 lines from the top) comparing enhancement with original profile (dotted line: original, solid line: enhanced).

In addition, Donoho [38] showed that if j_0 is a non-negative integer satisfying $2^{j0} > 2D + 2$ (defining non-interacting boundaries), then there exists a collection of functions $\phi_{j,k}^{interv}$ and $\psi_{j,k}^{interv}$ such that every $f \in \mathbf{C}$[0, 1] has a representation:

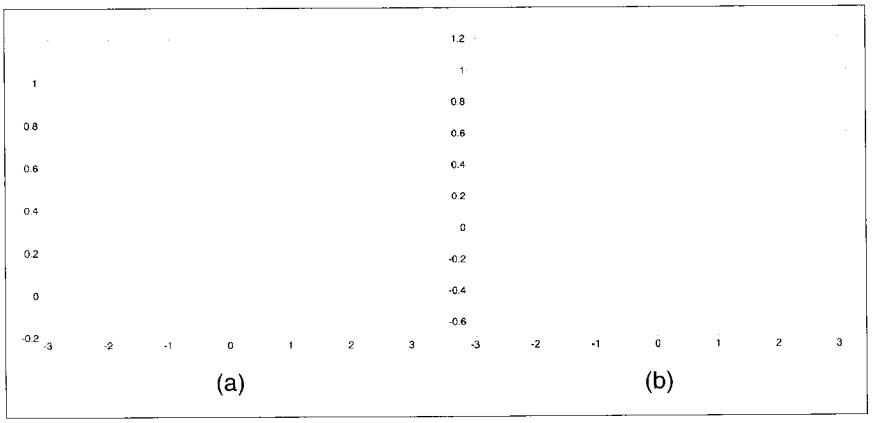

14. (a) Refinement relation for Deslauries-Dubuc interpolation. (b) Interval wavelet plot, $D = 3$.

Table 1: Filters for D= 3.*				
n	0	1	2	3
LEF_0 n	1.0000	0	0	0
LEF_1 n	0.3125	0.9375	-0.3125	0.0625
REF-2 -n	2.1875	-2.1875	1.3125	-0.3125
REF-1 -n	1.0000	0	0	0
* LEF = Left edge filter REF = Right edge filter				

Table 2: Interior Filter for D = 3								
n	0	1	2	3	4	5	6	7
IF(n)	-0.0625	0	0.5625	1.0000	0.5625	0	-0.0625	0

$$f = \sum_{k=0}^{2^{j_0-1}} S_j,k\phi_{j_0,k}^{interv} + \sum_{j\geq j_0}\sum_{k=0}^{2^{j-1}} d_{j,k}\psi_{j,k}^{interv}$$

with a uniform convergence of partial sums $j \leq j_1$ as $j_1 \rightarrow \infty$. For a detailed construction of $\phi_{j,k}^{interv}$ and $\psi_{j,k}^{interv}$ please refer to reference [38]. Tables 1 and 2 show the discrete filters used in our study for the case of $D = 3$. Figure 15 shows the boundaries of the associated interval wavelets. An example of the processing structures for the one dimensional case is shown is Fig. 16.

Enhancement Techniques

To accomplish multiscale contrast enhancement, both local and global techniques for image enhancement were applied to each multiresolution representation. For the interval wavelet basis, there were four components in the transform space: horizontal, vertical, diagonal, and a DC component, represented by d^i_1, d^i_3, d^i_3; s^i, respectively, where i is the transform level. Let s be the original mammogram, g be the function designed to emphasize features of importance within a selected level i, and L be the number of levels in a transform. Then an enhanced image may be given by:

$$\hat{s} = \sum_{i=1}^{L} W^{-1}\left(g\left(d_1^i\right), g\left(d_2^i\right), g\left(d_3^i\right), s^i\right) \quad (12)$$

In general, by defining a function g, we can denote specific enhancement schemes for modifying the coefficients within distinct levels of scale-space.

Local Enhancement Techniques

A problem for image enhancement in digital mammography is the ability to emphasize mammographic features while *reducing* the enhancement of noise. In [23-26] we presented a local enhancement technique for digital mammography based on multiscale edges. In this study, local enhancement was supported by:

$$\hat{d}_1^i(m,n) = \begin{cases} d_1^i(m,n), & \text{if } e^i(m,n) \leq T^i \\ g^i d_1^i(m,n), & \text{if } e^i(m,n) > T^i \end{cases}$$

where m and n denote d coordinates in the spatial domain, e^i was the edge set corresponding to transform space component d^i_1, g^i was a local gain, and T^i was a threshold at level i, g^i and T^i were selected adaptively. The edge set e^i of d^i_1 was the local maxima of d^i_1 along the horizontal direction. For d^i_2 and d^i_3, the direction was along the vertical and diagonal orientations (45°), respectively. Specifically:

$$e^i(m,n) = \begin{cases} \left|d_1^i(m,n)\right| & \text{if } \left|d_1^i(m,n)\right| > \left|d_1^i(m+1,n)\right| \text{ and } \left|d_1^i(m,n)\right| > \left|d_1^i(m-1,n)\right| \\ 0 & \text{otherwise} \end{cases}$$

The processing of d^i_2 and d^i_3 is similar. By replacing d^i_1; d^i_2 and d^i_3 in Eq. (1) with corresponding modified components $\hat{d}_1^i$, $\hat{d}_2^i$ and $\hat{d}_3^i$ we obtain an enhanced image $\hat{s}$.

Multiscale Adaptive Gain

In this approach, we suppressed pixel values of very small amplitude, and enhanced only those pixels that were larger than a certain threshold, T, within each level of transform space. We designed the following function to accomplish this non-linear operation [28]:

$$f(y) = a\left[\text{sigm}\left(c(y-b)\right) - \text{sigm}\left(-c(y+b)\right)\right] \quad (13)$$

where:

$$a = \frac{1}{\text{sigm}\left(c(1-b)\right) - \text{sigm}\left(-c(1+b)\right)}$$

$$0 < b < 1,$$

sigm(y) is defined by

$$\text{sigm}(y) = \frac{1}{1+e^{-y}}$$

$$\text{sigm}(y) = \frac{1}{1+e^{-y}}$$

and, b and c control the threshold and rate of enhancement, respectively. It can be easily shown that $f(y)$ is *continuous* and monotonically increasing within the interval [−1, 1] (similar to histogram equalization). Furthermore, a derivative of $f(y)$ of any order exists and is continuous. Therefore, enhancement accomplished by $f(y)$ will not introduce any new discontinuities (artifacts).

Experimental Results and Discussion

Preliminary results have shown that the multiscale processing techniques described above can make unseen or barely

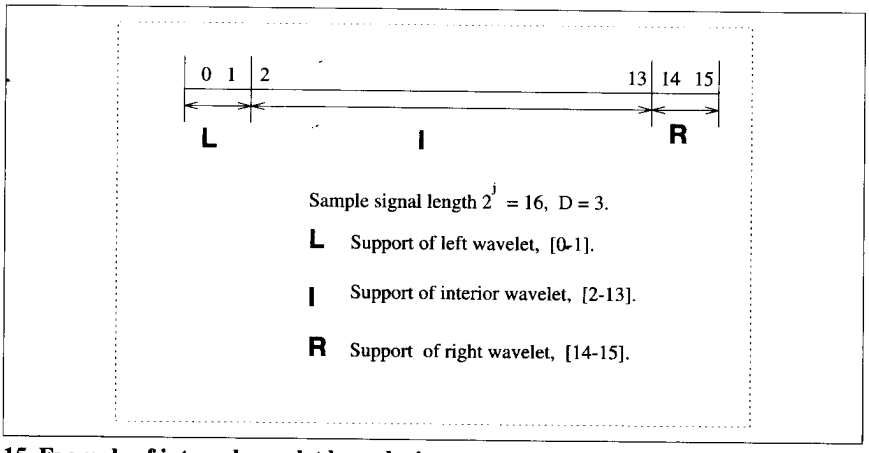

15. Example of interval wavelet boundaries.

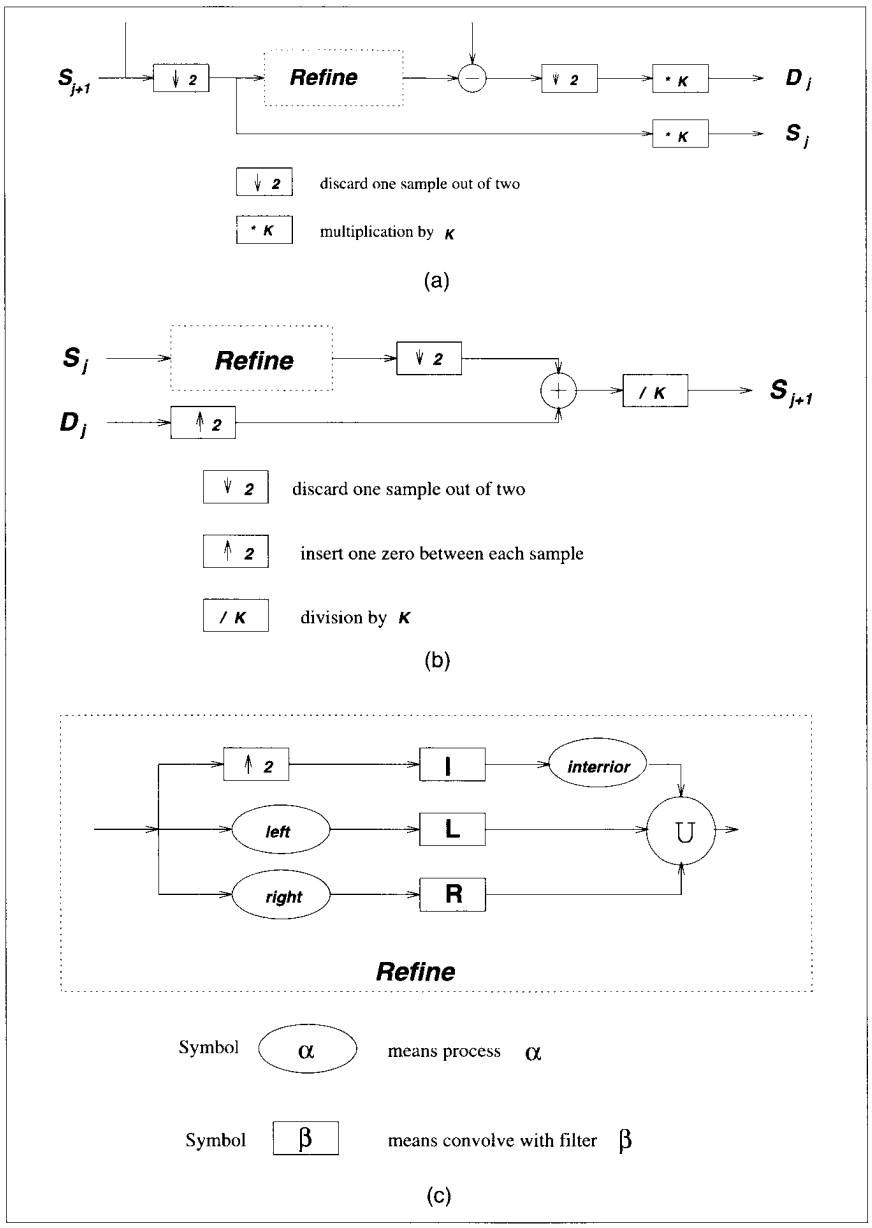

16. Processing overview for analysis and synthesis by interval wavelets. In the above diagrams, $K = \sqrt{2}$. For simplicity, only one-dimensional case is shown. (a) Decomposition structure. (b) Reconstruction structure. (c) Refinement processing structure.

seen features of a mammogram more obvious, without requiring additional radiation. Our study suggests that these techniques can improve the visualization of features of importance to mammography and assist the radiologist in the early detection of breast cancer.

Mathematical models of phantoms were constructed to validate our enhancement techniques against false positives arising from possible artifacts introduced and to evaluate contrast improvement quantitatively. Our models included features of regular and irregular shapes and sizes of interest in mammographic imaging, such as microcalcifications, cylindrical and spicular objects, and conventional masses. Techniques for "blending" a normal mammogram with the images of mathematical models were developed. The purpose of these experiments was to test the *performance* of our processing techniques on inputs known "a priori," using mammograms where the objects of interest were deliberately obscured by normal breast tissues. The "imaging" justification for "blending" is readily apparent; a cancer is visible in a mammogram because of its (slightly) higher X-ray attenuation, which causes a lower radiation exposure on the film in the appropriate region of a projected image.

Figure 18 (a) shows an example of a mammogram whereby the mathematical phantom shown in Fig. 18 (b) has been blended into a clinically-proven cancer-free mammogram Fig. 18 (a). The image shown in Fig. 18 (c) was constructed by adding the amplitude of the mathematical phantom image to the cancer free mammogram, followed by local smoothing.

Before applying our processing techniques, a computer simulated phantom was developed to both characterize and optimize each wavelet based enhancement algorithm [13], such as the levels of analysis, threshold (T) and gain (c) parameter values. This early study enabled us to compute an enhancement factor (EF), which was used to quantitatively measure algorithm performance. EF was defined as the ratio of output to input contrast noise ratios (CNR). The study found that computed EF values correlated well with the feature detection performance of radiologists.

In addition, radiologists at Shands Hospital at the University of Florida validated that processing the blended mammogram with our local enhancement techniques introduced no significant artifacts and preserved the shapes of the known mammographic features (calcifications, dominant masses, and spicular lesions) contained in the original mathematical phantom.

Enhancement by multiscale edges provided a significant improvement in local contrast for each feature included in the blended mammogram. A quantitative measure of contrast improvement can be defined by a contrast improvement index (CII), $\mathrm{CII} = \frac{C_{\mathrm{Processed}}}{C_{\mathrm{Original}}}$, where $C_{\mathrm{Processed}}$ and C_{Original} are the contrast values for a region of interest in the processed and original images, respectively.

In this paper we adopted a version of the optical definition of contrast introduced by Morrow, et al. [39]. The contrast C of an object was defined by $C = \frac{f-b}{f+b}$; where f was the mean gray-level value of a particular object in the image (*foreground*), and b was the mean gray-level value of a surrounding region (*background*). This definition of contrast has the advantage of being independent of the

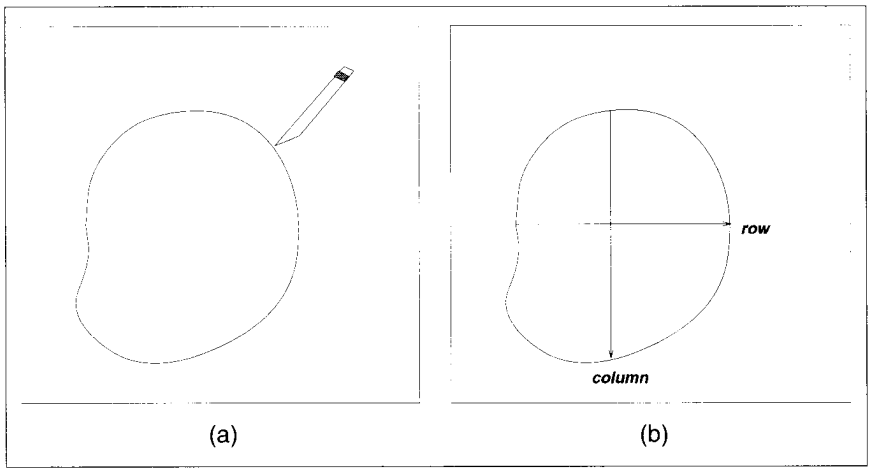

17. (a) Interactive selection of ROI by radiologist. (b) ROI is processed based on tensor product: each row is processed, followed by the processing of each column.

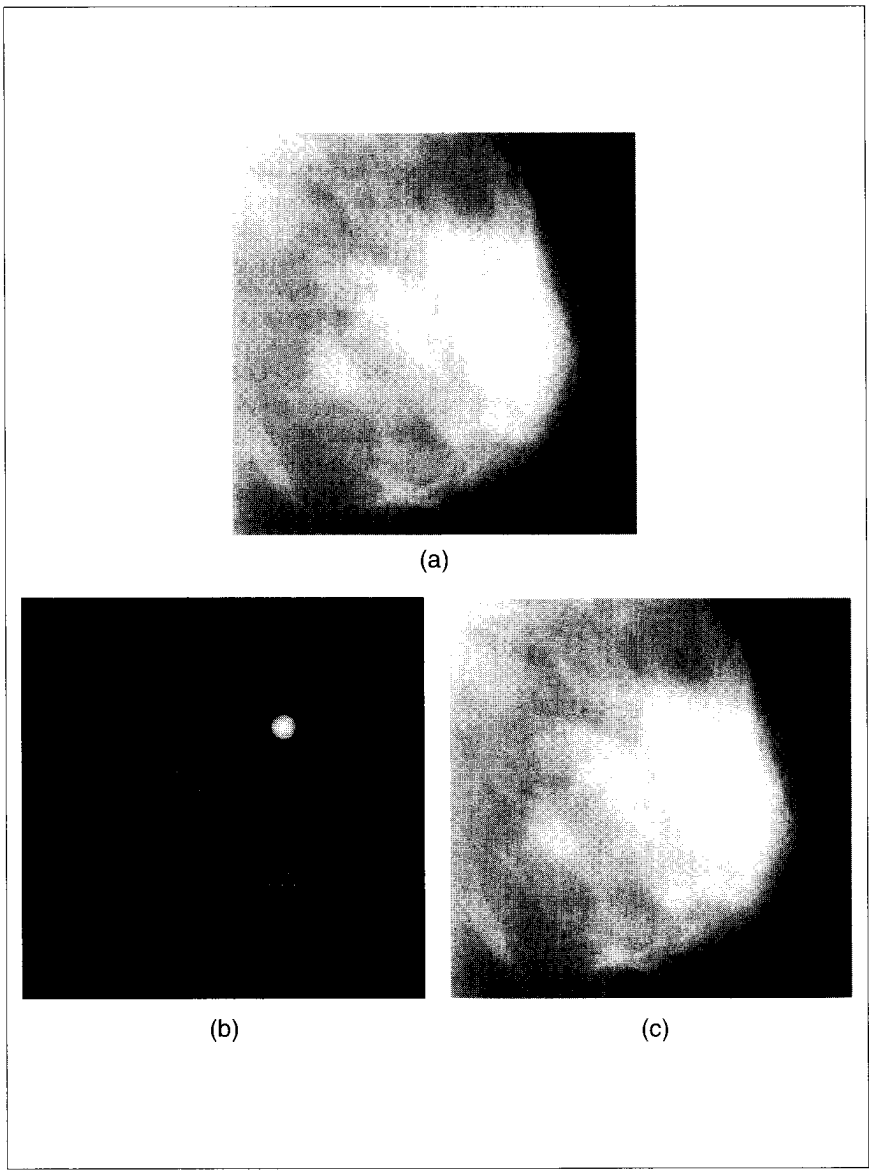

18. (a) Original dense mammogram, M56. (b) Mathematical phantom. (c) Mammogram M56 blended with phantom image.

actual range of gray levels in the image. For each feature included in the mathematical phantom, local masks were defined to separate the foreground and background regions of each feature in the blended mammogram.

Figure 19 (a) shows the result after processing the blended mammogram with adaptive histogram equalization (AHE). Figure 19 (b) was obtained after reconstructing the blended mammogram from interval wavelet transform coefficients modified by multiscale adaptive gain processing (GAIN). Figure 19 (c) shows the result after processing the blended mammogram with unsharp masking (UNS). Figure 19 (d) shows the result obtained after reconstructing the blended mammogram from interval wavelet transform coefficients modified by multiscale edges (EDGE). Figure 20 shows enlarged areas (16*X*) containing each feature in the processed mammogram for each method of contrast enhancement. The images in each row of Fig. 20 were rescaled by the same linear transformation.

Table 3 shows the contrast values for the original and enhanced mammographic features shown in Fig. 19, while Table 4 shows the values for CII. From the two tables, we observed that both GAIN and EDGE enhancement methods performed significantly better than unsharp masking (UNS) and adaptive histogram equalization (AHE).

Figure 21 demonstrates the improvement of local contrast accomplished by GAIN for a sample scan line profile taken from cross sections of each features. Figure 22 shows the improvement of local contrast for the same scan line accomplished by the EDGE method. Note that in all cases contrast was improved while preserving the overall shape of each feature profile.

By applying wavelets constructed on the interval, we can more efficiently accomplish enhancement of an arbitrary region of interest (ROI) of a digital mammogram. Figure 23 (a) shows the enhancement of an arbitrary region of interest using adaptive gain processing of a DD interval wavelet interpolation basis. Figure 23 (b) shows the enhancement of an arbitrary region of interest using multiscale edges of the same interval wavelet basis. The decomposition of the selected ROI was computed by processing horizontal and vertical "scan lines." Enhancement was then achieved by modifying only the coefficients within the ROI, and then simply reconstructing.

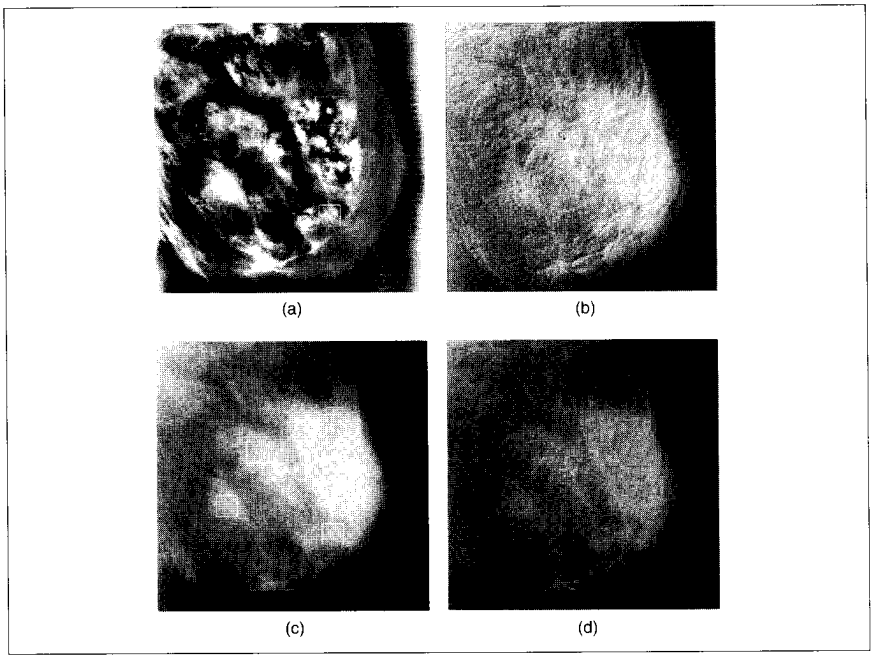

19. Blended mammogram: (a) Enhancement by adaptive histogram equalization, (b) Enhancement by adaptive gain processing of DD interpolation coefficients, (c) Enhancement by traditional unsharp masking, (d) Enhancement by multiscale edges of DD interpolation coefficients.

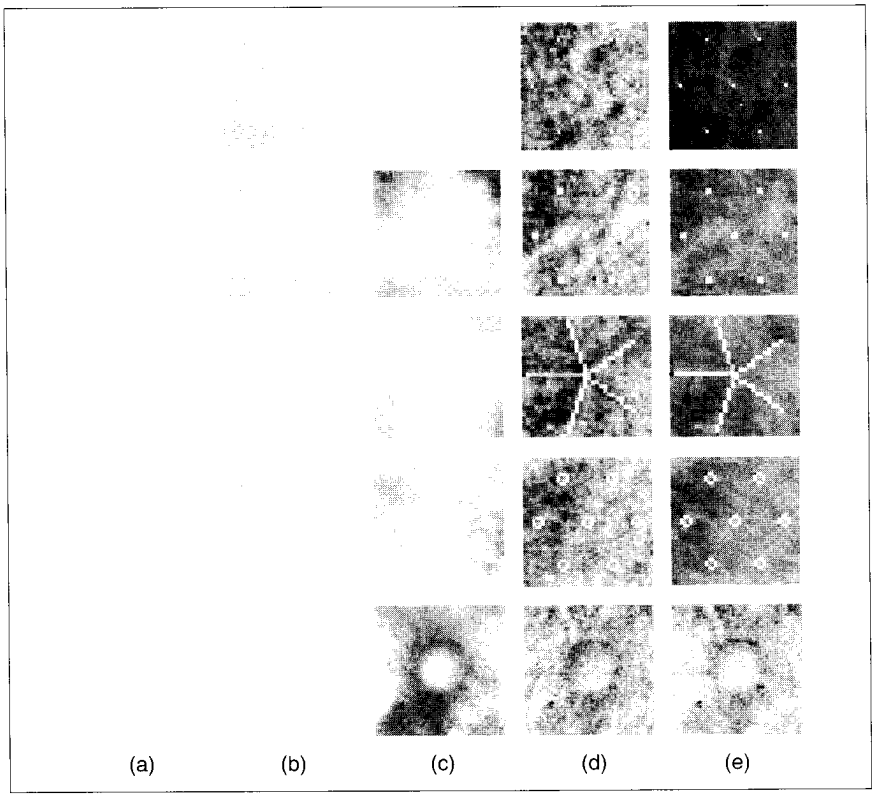

20. Contrast enhancement of features in blended mammogram. Phantom mammographic features from top to bottom: minute microcalcification cluster, microcalcification cluster, spicular lesion, circular (arterial) calcification, and a well-circumscribed mass. (a) Original image. (b) Enhancement by unsharp masking. (c) Enhancement by adaptive histogram equalization. (d) Enhancement by adaptive gain processing of DD wavelet coefficients. (e) Local enhancement by multiscale edges of DD wavelet coefficients.

By constraining the enhancement to a specific region, computation costs were greatly reduced. For example, Table 5 shows the comparison of actual computation time for processing an entire mammogram (complete image matrix) versus a selected ROI.

In summary, methods for accomplishing adaptive contrast enhancement by a multiscale representation were investigated. Contrast enhancement was applied to features of specific interest to mammography including masses, spicules and microcalcifications. Multiresolution representations provided an adaptive mechanism for the local emphasis of such features blended into digitized mammograms. In general, improvements in image contrast based on multiscale processing were superior to those obtained using competitive algorithms of unsharp masking and adaptive histogram equalization.

Using Deslauriers-Dubuc interpolation interval wavelets, we demonstrated the enhancement of arbitrary regions of interest. This can provide radiologists with an interactive capability for enhancing only suspicious regions of a mammogram, at a reduced computational cost.

Conclusion

In both studies above, multiresolution representations provided an adaptive mechanism for the local emphasis of features of importance to mammography. In general, improvements in image contrast for multiscale image processing algorithms were superior to those obtained using existing competitive algorithms. These initial results are encouraging and suggest that wavelet based image processing algorithms could play an important role in improving the imaging performance of digital mammography.

In Part 2, features blended into the mammograms were "idealized" representations of the types of objects that are of primary interest to mammographers. The resultant mammographic images were appropriate for the purpose of demonstrating improved image contrast made possible by wavelet based image processing algorithms. These images were also useful for comparing multiscale wavelet based algorithms with existing image processing algorithms. The test results obtained in this study, however, cannot be directly extrapolated to clinical mammography. In addition, it is also important to study possible image artifacts introduced

Table 3: Contrast Values*					
Feature	**$C_{original}$**	**C_{UNS}**	**C_{AHE}**	**C_{GAIN}**	**C_{EDGE}**
Minute micrcalcification cluster	0.0507	0.0674	0.0428	0.3952	0.6454
Microcalcification cluster	0.0332	0.1227	0.1652	0.3626	0.3678
Spicular lesion	0.0287	0.0579	0.1025	0.3608	0.3949
Circular (arterial) calcification	0.0376	0.0823	0.1677	0.3014	0.4021
Well-circumscribed mass	0.0035	0.0052	0.1091	0.0344	0.0397

*$C_{original}$ for features in the orignal blended mammorgram M56, C_{UNS} for enhancement by unsharp masking, C_{AHE} for enhancement by adaptive histogram equalization, C_{EDGE} for enhancement by multiscale edges obtained from Deslauriers-Dubuc interpolation (EDGE), and C_{GAIN} for global enhancement by adaptive gain processing of Deslauriers-Dubuc interpolation (GAIN).

Table 4: Contrast Improvement Index*				
Feature	**CII_{UNS}**	**CII_{AHE}**	**CII_{GAIN}**	**CII_{EDGE}**
Minute microcalcification cluster	1.3294	0.8842	7.7949	12.7298
Microcalcification cluster	3.6958	4.9759	10.9217	11.0783
Spicular lesion	2.0174	3.5714	12.5714	13.7596
Circular (arterial) calcification	2.1888	4.4601	8.0160	11.3429
Well-circumscribed mass	1.4857	31.1714	9.8286	11.3429

* CII for enhancement by unsharp masking (UNS), adaptive histogram equalization (AHE), and by local enhancement of multiscale edges obtained from Deslauriers-Dubuc interpolation (GAIN).

Table 5: Computation Costs*			
Matrix size (number of pixels)	**T_{matrix}**	**T_{ROI}**	**T_{matrix}/T_{ROI}**
512 x 512	748	135	5.54
1024 x 1024	5760	135	42.67

*in seconds. T_{matrix} represents the time required to process an entire mammogram, while T_{ROI} represents the time to process only a selected ROI. The number of pixels within the ROI shown in Fig. 12 was 76,267. The program was executed on the Sun SparcStation Model 10/30.

by new wavelet filters, which may increase the false positive rate.

Thus, it is essential that further studies be performed to identify the most promising approaches of multiscale based image processing algorithms. The identification of the most appropriate basis functions for enhancing specific types of mammographic features needs further investigation. The best way of selecting wavelet coefficients for enhancement, and their degree of enhancement, also merit systematic analysis. Ultimately, however, the objective of any image processing is to improve the visibility of clinically significant feature. Accordingly, the most promising algorithms require clinical evaluation. In the near future, such tests will be designed to measure the ability of multiscale image processing to significantly improve the sensitivity, specificity and overall accuracy of mammographic interpretation.

Acknowledgments

This work was sponsored in part by the Whitaker Foundation and the U.S. Army Medical Research and Development Command, Grant No. DAMD17-93-J-3003. Special thanks to Dr. Walter Huda and Sergio Schuler for their assistance in metrics for the evaluation of contrast performance.

Andrew Laine received DSc and MSc degrees from Washington University (St. Louis) School of Engineering and Applied Science in Computer Science, 1989 and 1983 respectively, and BS degree from Cornell University (Ithica). He joined the Department of Computer and Information Sciences

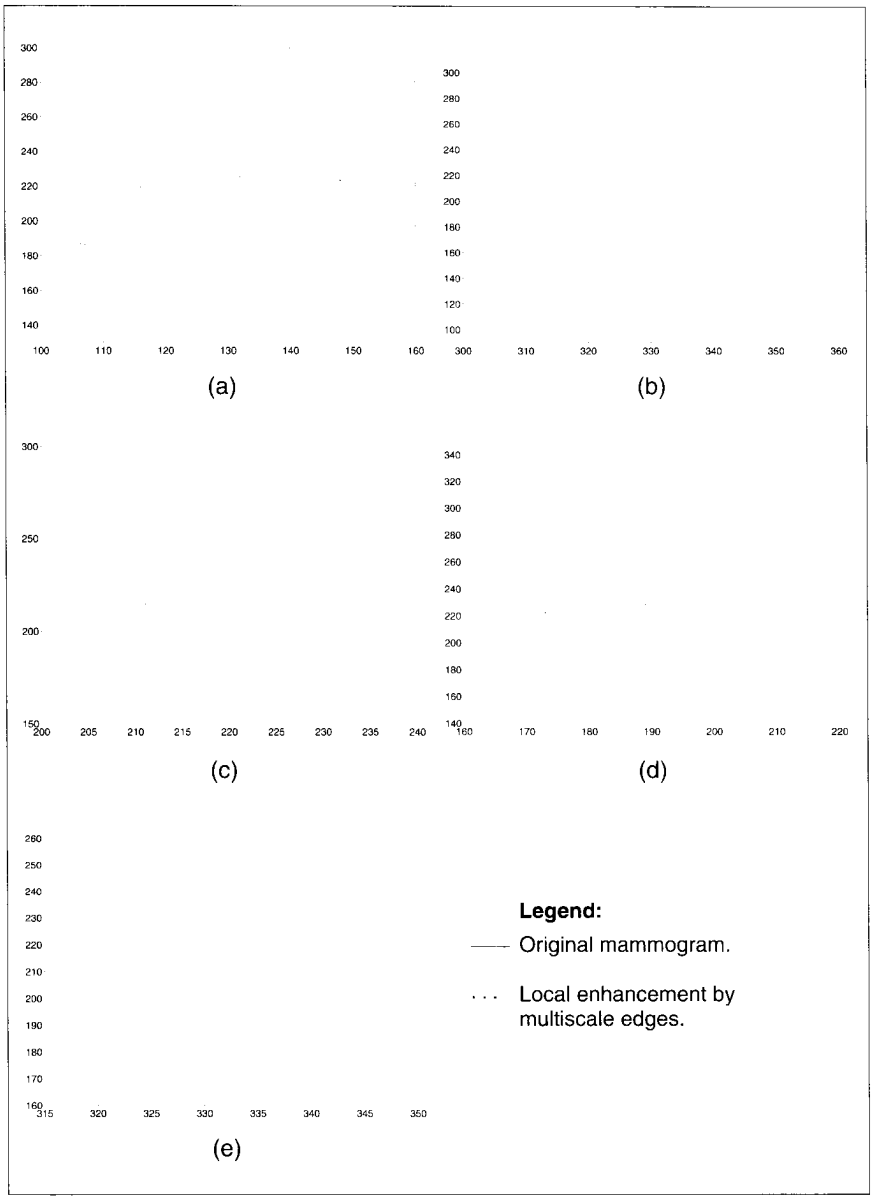

21. Sample scan lines displaying enhancement by the method of adaptive gain processing of DD wavelet coefficients: (a) minute microcalcifications cluster, (b) microcalcification cluster, (c) spicular lesion, (d) circular (arterial) calcification and (e) well-circumscribed mass.

and Engineering at the University of Florida, Gainesville, in 1990, and is now an Associate Professor.

His research interests include methods of multiresolution analysis applied to problems in computer vision, pattern recognition, medical imaging, and applied mathematics. Dr. Laine served as guest editor for the Journal of Mathematical Imaging and Vision special issue on Wavelet Theory and Application, in March 1993, and has edited the book, "Wavelet Theory and Applications," Kluwer, 1995. He has chaired the annual SPIE conference on "Wavelet Application in Signal and Image Processing", San Diego, CA, in the years 1993-1995.

In addition, Professor Laine has coauthored chapters in the books "Wavelet Applications in Medicine and Biology", CRC Press, 1995, and "Time Frequency and Wavelets in Biomedical Engineering," IEEE Press, 1995. He also served on the program committee for the IEEE-EMBS Workshop on Wavelet Applications in Medicine in 1994. Dr. Laine is member of the IEEE Computer Society and Engineering in Medicine and Biology Society.Address for correpsondence: Department of Computer and Information Science and Engineering, University of Florida, Gainesville, FL 32611. E-mail: Laine@cis.ufl.edu. Tel: (904) 392-1239

Jian Fan received BS and MS degrees in Physics from Xiamen University, PR China in 1982 and 1985 respectively. Prior to entering the PhD program at the University of Florida (Gainesville) he was an instructor at Xiamen University from 1985-89. Mr. Fan received his MS degree in Computer and Information Sciences in 1992. His research interest include image processing, feature analysis and pattern recognition. He is currently a member of technical staff at Hewlett-Packard, San Diego, CA.

Wuhai Yang received his BS and MS degrees in electrical engineering from Wuhan University of PR China in July, 1986, and July, 1989, respectively. Prior to pursuing graduate studies within the Department of Computer and Information Sciences and Engineering at the University of Florida (Gainesville), he was a software engineer for the Beijing-Guandong Chinese Computer Center, July, 1989 through December, 1992.

In December of 1994, he received the Master of Science degree in Computer and Information Sciences from the University of Florida, Gainesville. He is currently a software system engineer for Applied Digital Technology, Inc. in Gainesville, FL.

References

[1] R.A. Smith, "epidemiology of breast cancer" in *A categorical course in physics. Technical aspects of breast imaging*, A.G. Haus and M.J. Yaffe, Eds. Radiological Society of North America, 1993, pp. 21-33, Presented at the 79th scientific assembly and annual meeting of the RSNA.

[2] P.C. Johns and M.J. Yaffe. "X-ray characterization of normal and neoplastic breast tissues" *Physics in Medicine and Biology*, Vol. 32, No. 6, pp. 675-695, Feb. 1987.

[3] M.J. Yaffe and R.J. Jennings and R. Fahrig and T.R. Fewell. "X-ray spectral considerations for mammography" in *A categorical course in physics. Technical aspects of breast imaging*, A.G. Haus and M.J. Yaffe, Eds. Radiological Society of North America, 1993, pp. 63-72, Presented at the 79th scientific assembly and annual meeting of the RSNA.

[4] I. Brodie and R.A. Gutcheck. "radiographic

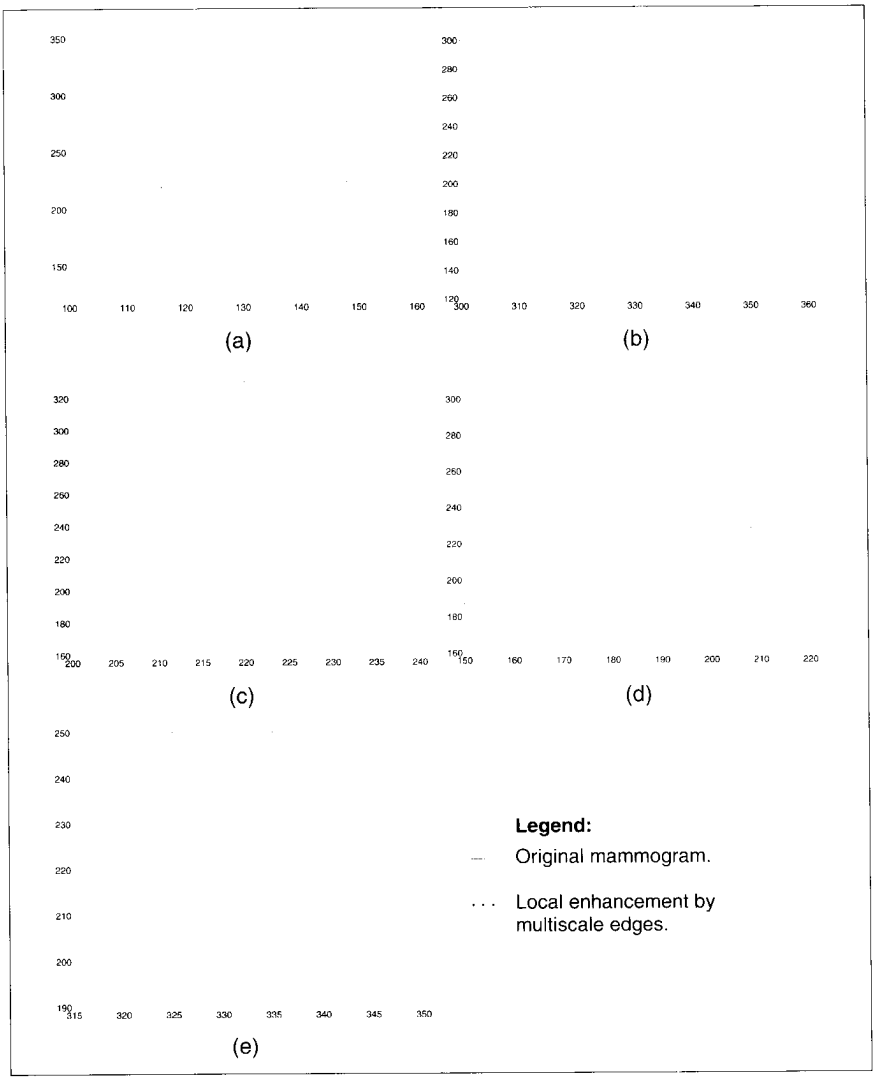

22. Sample scan lines displaying enhancement by the method of multiscale edges of DD wavelet coefficients: (a) minute microcalcification cluster, (b) microcalcification cluster, (c) spicular lesion, (d) circular (arterial) calcification and (e) well-circumscribed mass.

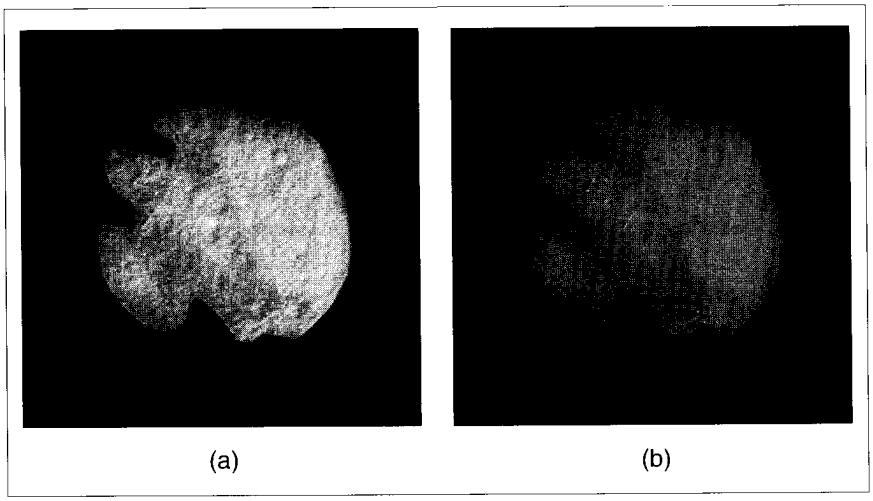

23. ROI enhancement of the blended mammogram shown in Figure 18 (c). (a) ROI enhancement by adaptive gain processing of DD wavelet coefficients. (b) ROI enhancement by multiscale edges of DD interpolation.

information theory and application to mammography" *Medical Physics*, Vol. 9, 1982.

[5] R. Gorden, R.M. Rangayyan, "feature enhancement of film mammograms using fixed and adaptive neighborhoods," *Applied Optics*, Vol. 23, pp. 560, 1984.

[6] A.P. Dhawan, G. Buelloni, R. Gordon, "enhancement of mammographic features by optimal adaptive neighborhood image processing," *IEEE Transactions on Medical Imaging*, Vol. MI-5, pp. 8, 1986.

[7] A.P. Dhawan, R. Gordon, "reply to comments on enhancement of mammographic features by optimal adaptive neighborhood image processing," *IEEE Transactions on Medical Imaging*, Vol. MI-6, pp. 82, 1987.

[8] A.P. Dhawan, E. Le Royer, "mammographic feature enhancement by computerized image processing," *Computer Methods and Programs in Biomedicine*, Vol. 27, pp. 23, 1988.

[9] P.G. Tahoces, J. Correa, M. Souto, C. Gonzalez, L. Gomez, J. Vidal, "Enhancement of chest and breast radiographs by automatic spatial filtering," *IEEE Transaction on Medical Imaging*, Vol. MI-10(3), pp. 330-335, 1991.

[10] D. Brzakovic and X.M. Luo and P. Brzakovic, "an approach to automated detection of tumors in mammograms," *IEEE Transaction on Medical Imaging*, Vol. 9, No. 3, pp. 232-241, Sept. 1990.

[11] H.P. Chan and K. Doi and S. Galhotra and C.J. Vyborny and H. MacMahon and P.M. Jokich, "image feature analysis and computer-aided diagnosis in digital radiography. automated de- tection of microcalcifications in mammography," *Medical Physics*, Vol. 14, No. 4, pp. 538-548, July, 1987.

[12] H.P. Chan and K. Doi and C.J. Vyborny and K.L. Lam and R.A. Schmidt, "Computer-aided detection of microcalcifications in mammograms: Methodology and preliminary clinical study," *Investigative Radiology*, Vol. 23, No. 9, pp. 664-671, Sept. 1988.

[13] Y. Xing, W. Huda, A. Laine, "Simulated phantom images for optimizing wavelet based image processing algorithms in mammography," *Proceedings of SPIE-The International Society for Optical Engineering*,Vol. 2299, pp. 207-217, July, 1994.

[14] T.N. Wiesel. "postnatal development of the visual cortex and the influence of environment" *Nature*, Vol. 299, No. 5883, pp. 583-591, Oct. 1982.

[15] D. C. Wang, A. H. Vagnucci and C. C. Li. "digital image enhancement: a survey" *Computer Vision, Graphics, and Image Processing*, Vol. 24, 363-381, 1983.

[16] R. Hummel. "histogram modification techniques" *Computer Graphics and Image Processing*, Vol. 4, pp. 209-224, 1975.

[17] W. Frei. "image enhancement by histogram hyperbolization" *Computer Graphics and Image Processing*, Vol. 6, pp. 286-294, 1977.

[18] S. M. Pizer, E. P. Amburn, et al. "adaptive histogram equalization and its variations" *Computer Vision, Graphics, and Image Processing*, Vol. 39, 355-368, 1987.

[19] A. Rosenfeld and A.C. Kak. "digital picture

processing" *Academic Press, Second edition*, New York, 1982.

[20] L.D. Loo, K. Doi and C.E. Metz. "investigation of basic imaging properties in digital radiograpgy. 4. effect of unsharp masking on the detectability of simple patterns" *Med. Phys.*, 12(2), pp. 209-214, 1985.

[21] F. Neycenssac. "contrast enhancement using the Laplacian-of-a-Gaussian filter" *CVGIP: Graphical Models and Image Processing*, Vol. 55, No. 6, pp. 447-463, 1993.

[22] A. Beghdadi and A. L. Negrate. "contrast enhancement technique based on local detection of edges" *Comput. Vision Graphics Image Process.* 46, pp. 162-174, 1989.

[23] A. Laine. Multiscale wavelet representations for mammographic feature analysis. In *Image Enhancement Techniques: Computer Science, National Cancer Institute Breast Imaging Workshop: State-of-the-Art and New Technologies*, Bethesda, MD, September 1991.

[24] A. Laine, S. Song. Multiscale wavelet representations for mammographic feature analysis. In *Proceedings of SPIE: Conference on Mathematical Methods in Medical Imaging*, San Diego, CA, July 23-25, 1992.

[25] A. Laine, S. Song. Wavelet processing techniques for digital mammography. In *Proceedings of SPIE: Conference on Visualization in Biomedical Computing*, Chapel Hill, NC, October 13-16, 1992.

[26] A. Laine, S. Song, J. Fan. Adaptive Multiscale Processing for Contrast Enhancement. In *Pro-ceedings of SPIE: Conference on Biomedical Imaging and Biomedical Visualization*, San Jose, CA, January 31-February 4, 1993.

[27] B. D. Jawerth, M. L. Hilton and T. L. Huntsberger. Local enhancement of compressed images. *J. Mathematical Imaging and Vision*, Vol. 3 , pp. 39-49, 1993.

[28] A. Laine, S. Schuler, J. Fan, W. Huda. Mammographic feature enhancement by multiscale analysis. *IEEE Trans. on Medical Imaging*, Vol. 13, No. 14, pp. 725-740, Dec. 1994.

[29] J. Lu and D.M. Healy Jr. Contrast enhancement of medical images using multiscale edge representation. In *Proceedings of SPIE: Wavelet applications*, Orlando, FL, April 5-8, 1994.

[30] S.Mallat. "a theory for multiresolution signal decomposition : the wavelet representation." *IEEE Trans. Pattern Anal. Machine Intell.*, vol. PAMI-11, pp. 674-693, 1989.

[31] S.Mallat and Sifen Zhong. "characterization of signals from multiscale edges." *IEEE Trans. Pattern Anal. Machine Intell.*, vol. PAMI-14, pp. 710-732, 1992.

[32] S.Mallat and W. L. Hwang. "sigularity detection and processing with wavelets." *IEEE Trans. Inform. Theory*, Vol.38, NO. 2, pp. 617-643, 1992.

[33] D. L. Donoho. "nonlinear wavelet methods for recovery of signals, densities, and spectra from indirect and noisy data" *Proc. Symposia Applied Math.* , Vol. 0, 1993

[34] Jian Fan and A. Laine. "contrast enhancement by multiscale and nonlinear operators," Technical report, University of Florida, 1994.

[35] G. Deslauriers, S. Dubuc, "Symmetric iterative interpolation process," *Constructive Approximation*, vol. 5, pp. 49-68, 1989.

[36] S. Dubuc, "Interpolation through an iterative scheme," *J. Math. Anal. and Appl.*, vol. 114, pp. 185-204, 1986.

[37] A. Cohen, I. Daubechies, "Wavelets on the interval and fast wavelet transforms," *Applied and Computational Harmonic Analysis*, Vol. 1(1), pp. 54-81, 1993.

[38] D. L. Donoho, "Smooth wavelet decomposition with blocky coefficient kernels," *Recent Advances in Wavelet Analysis*, pp. 1-43, Academic Press , Inc., Boston, 1994.

[39] W. M. Morrow, R.B. Paranjape, R.M. Rangayyan, J.E.L. Desautels. Region-based contrast enhancement of mammograms. *IEEE Transactions on Medical Imaging*. Vol. 11(3): 392-406, 1992.

[40] L. Anderson, N Hall, B. Jawerth, and G. Peters, "Wavelets on closed subsets of the real line," *Topics In the Theory and Applications of Wavelets*, Larry L. Schumaker and Glenn Webb, Eds, Academic Press, Boston.